applied sciences

MDPI

Article

Experimental Forced Convection Study Using a Triply Periodic Minimal Surface Porous Structure with a Nanofluid: Comparison with Numerical Modeling

Mohamad Ziad Saghir [1,*] and Gulenay Alevay Kilic [2]

[1] Department of Mechanical Engineering, Toronto Metropolitan University, Toronto, ON M5B 2K3, Canada
[2] Electric and Energy Department, Yalova University, Yalova 77200, Türkiye; gulenay.kilic@yalova.edu.tr
* Correspondence: zsaghir@torontomu.ca

Abstract: Triply periodic minimal surfaces (TPMSs) show potential as porous materials in different engineering applications. Amongst them, heat sink is the subject of this paper. The advantage of such a structure is the ability to design it based on the intended applications. In the present paper, an attempt is made to experiment with a better understanding of the performance of TPMSs in heat sink applications. The experiment was conducted for different flow rates, and two heat sink materials, aluminum and silver, were used. In addition, two fluids were used experimentally: The first was water, and the second was a mixture of water containing 0.6% aluminum nanoparticles and identified as a nanofluid. The applied heat flux was maintained constant at 30,800 W/m^2. The results reveal experimentally and confirm numerically that the TPMS structure secures a uniform heat extraction in the system. The development of the boundary layer in the porous structure is reduced due to the current structure design. A higher Nusselt number is obtained when the nanofluid is used as the circulating fluid. The performance evaluation criteria in the presence of the nanofluid exceed 100.

Keywords: TPMS; nanofluid; water; porous structure; convection; experimental measurements

check for updates

Citation: Saghir, M.Z.; Kilic, G.A. Experimental Forced Convection Study Using a Triply Periodic Minimal Surface Porous Structure with a Nanofluid: Comparison with Numerical Modeling. *Appl. Sci.* **2024**, *14*, 7594. https://doi.org/10.3390/app14177594

Academic Editors: Marco Azzolin, Andrea Diani and Luca Viscito

Received: 1 August 2024
Revised: 21 August 2024
Accepted: 22 August 2024
Published: 28 August 2024

Copyright: © 2024 by the authors. Licensee MDPI, Basel, Switzerland. This article is an open access article distributed under the terms and conditions of the Creative Commons Attribution (CC BY) license (https://creativecommons.org/licenses/by/4.0/).

1. Introduction and Literature Review

Integrating triply periodic minimal surfaces (TPMSs) with additive manufacturing technologies has emerged as a promising frontier in advanced thermal management and heat transfer systems. This innovative approach addresses the escalating demands of next-generation power plants and high-performance thermal applications. TPMS structures, characterized by their unique geometric properties and ability to create interpenetrating channels, offer significant potential for enhancing heat transfer efficiency while minimizing pressure drop. Recent research has explored various TPMS geometries, their fluid dynamic characteristics, and their application in heat exchangers and sinks. This work encompasses experimental studies, numerical simulations, and theoretical analyses, aiming to optimize TPMS designs for improved thermal performance across various operating conditions and fluid types, including nanofluids.

Dutkowski et al. [1] conducted a comprehensive review, highlighting the potential of minimal surfaces, especially TPMSs, in heat transfer applications. Abueidda et al. [2] analyzed TPMS structures' potential in heat transfer applications. They examined the geometric properties of TPMS structures, analyzed their effects on heat transfer and fluid flow, and compared the performance of different TPMS types. Their study demonstrated the advantages of TPMS structures over conventional porous materials and evaluated their heat transfer efficiency using numerical simulations.

Al-Ketan et al. [3] focused on the performance of TPMS-based heat sinks, investigating the use of various TPMS geometries as heat sinks. They examined the effects of parameters such as porosity and surface area on heat transfer, explicitly evaluating performance metrics

like pressure drop and heat transfer coefficient for TPMS structures. By combining experimental and numerical methods, this comprehensive study demonstrated the superiority of TPMS-based heat sinks over traditional fin structures and emphasized the potential benefits of optimized TPMS designs in heat management applications.

Regarding fluid dynamics and heat transfer, Yang et al. [4] presented an extensive analysis to understand the effects of TPMS structures' complex geometry on fluid dynamics and heat transfer. The study examined various TPMS types (e.g., gyroid, diamond, and primitive) and investigated their flow guidance, turbulence generation, and heat transfer surface enhancement properties. Using computational fluid dynamics (CFD) simulations, the researchers evaluated the performance of TPMS structures at different Reynolds numbers and heat fluxes. The results indicated that the TPMS structures provided higher heat transfer coefficients and lower pressure drops than conventional flat channels, with the gyroid structure exhibiting the best thermo-hydraulic performance. The study also revealed that the TPMS structures enhanced heat transfer by increasing flow mixing and inhibiting boundary layer formation.

Tijing et al. [5] reviewed 3D printing for membrane separation, desalination, and water treatment. They indicated that 3D printing has a high potential for various engineering applications.

Peng et al. [6] investigated a novel approach beyond current heat exchanger designs, considering the high-temperature operating requirements of next-generation power plants. The study focused on combining TPMSs with additive manufacturing technology. The ability of TPMSs to separate three-dimensional space into two interpenetrating channels was examined, and it was found that this structure provided a high surface area-to-volume ratio with a low hydrodynamic resistance. It was observed that simple implicit functions with parameters such as periodic length and offset parameters could govern the design of TPMS heat exchangers. Furthermore, a numerical model was developed to optimize the performance of these heat exchangers. The produced prototype was experimentally tested, and its performance was evaluated.

Baobaid et al. [7] examined fluid flow and heat transfer in porous heat sinks with TPMS structures under free convection conditions. They addressed this using TPMS structures as heat sinks, focusing mainly on gyroid, diamond, and primitive TPMS structures. This approach aligns with the works of Al-Ketan et al. [3] and Abueidda et al. [4]. Saghir et al. [8] compared the thermal and hydraulic performance of porous block and gyroid structures. These structures, produced using 3D-printing technology, were investigated through experimental methods and numerical simulations using the COMSOL Multiphysics software, version 6. The research revealed that the gyroid structure provided a better thermal performance and lower pressure drop. The complex geometry of the gyroid was reported to enhance heat transfer by extending the flow path and increasing turbulence. With increasing flow rates, the heat transfer coefficient increased in both structures, but the gyroid structure was observed to provide a more uniform temperature distribution. These findings suggested that TPMS structures, especially the gyroid geometry, could be more advantageous in heat sink applications than conventional porous structures.

Moradmand and Sohankar [9] investigated the thermo-hydraulic performance of heat exchangers with Schwarz-P and gyroid structures, analyzing TPMS structures with different porosity ratios using numerical and experimental methods. The results showed that the gyroid structure provided a higher heat transfer performance and lower pressure drop than the Schwarz-P one. They increased the porosity ratio and thus enhanced heat transfer while reducing pressure drop. An increase in the Reynolds number was reported to increase both the heat transfer coefficient and pressure drop. The study demonstrated that the gyroid geometry exhibited a better thermo-hydraulic performance than conventional heat exchangers and could offer significant advantages in energy efficiency and compact heat exchanger design. Hu et al. [10] investigated flow characteristics in metal foams using experimental and numerical methods. Airflow through metal foams of varying porosities was analyzed using particle image velocimetry (PIV) technique and Computational Fluid

Dynamics (CFD) simulations. The research results showed that, as the porosity of metal foams increased, the flow resistance decreased, while lower porosity foams generated a higher turbulence intensity. The complex structure of metal foams was observed to enhance heat transfer by extending the flow path and increasing turbulence. Increasing the Reynolds number was found to improve the turbulence intensity and heat transfer. The study emphasized that the structural properties of metal foams significantly affect the flow characteristics and heat transfer performance, providing insights for optimizing the use of metal foams in applications such as heat exchangers and heat sinks.

Alqarni et al. [11] numerically observed that the presence of grooves inside the pipe of a heat exchanger has a significant effect on increasing the efficiency. Additionally, it was demonstrated that using nanofluids enhances the heat exchanger's energy efficiency. Furthermore, four different grid models were developed to select the optimum grid (GM) with the least computation time and highest accuracy. Eshgarf et al. [12] examined various types of heat exchangers used in the industrial and engineering fields to increase the heat transfer rate (HTR). The article discussed active, passive, and hybrid heat transfer enhancement techniques, mentioning using nanofluids as one of the passive methods to increase the HTR. The governing equations of nanofluid flows were presented, comparing single-phase models (SPMs) and two-phase models (TPMs). Their analysis did not conclusively verify which model is superior.

Tang et al. [13] investigated the convective heat transfer performance of TPMS structures used to develop high heat-dissipating devices. The TPMS structures examined were gyroid, diamond, and Iwp, and their performance was compared with a fins structure. An experiment was conducted to validate the accuracy of the numerical simulation. The results showed a good agreement between the simulation and experiment with an error margin of less than 6%. Among the three TPMS structures, TPMS-Diamond was concluded to have the best convective heat transfer performance due to its geometric structure without "holes", thus causing the wall to disturb the fluid more and enhance heat transfer.

Ho et al. [14] experimentally investigated the thermal performance of a microchannel heat sink (MCHS) using a nanofluid. The heat dissipation performance of pure water and the nanofluid on MCHS was studied. It was reported that microchannel heat sinks can be widely used in electronic devices to provide high heat dissipation rates and optimal performance with durability. Rathore et al. [15] examined flow and heat transfer in porous media. Porous structures created using lattice-shaped TPMS (diamond, I-WP, primitive, and gyroid) were analyzed. The research focused on the effects of shape morphology, tortuosity, micro-porosity, and effective porosity on the permeability and inertial drag factor. Using numerical simulations, conductivity and inertial drag coefficient values were determined for different flow regimes and structure types. The results provide essential insights for understanding and optimizing flow behavior in porous media.

Vahedi et al. [16] aimed to improve the performance and reduce the cost of heat exchangers in oil refineries. Analyses using two different oil-based nanofluids (MgO-SAE10 and ZnO-SAE10) revealed significant improvements in the thermal–hydraulic performance of heat exchangers, ranging from 84.78% to 107.68%. The findings demonstrated that using nanofluids in heat exchangers is advantageous in terms of both performance and cost. These research efforts indicate that minimal surfaces, particularly TPMS structures, have a wide range of applications in heat transfer systems for developing more efficient designs. The effects of different fluids, materials, and structural designs on heat transfer performance are being examined in detail, providing valuable insights for future advancements in this field.

The literature review shows that the experimental measurement of the TPMS structure in heat removal is not well spread. Many numerical modelling papers have been published, but experimental measurement is crucial in investigating the importance of this class of porous structure. Kerme et al. [17] recently showed the importance of implementing this new class of TPMS porous structure for heat enhancement. As stated by the authors, one of the unique experimental findings is the uniformity of the temperature distribution. That means the buildup of the thermal boundary layer is minimal. This is due to the connectivity

channels, which, in some cases, break this boundary layer. In this article, Kerme et al. [17] used distilled water as the cooling fluid and investigated experimentally different classes of TPMS structures having different porosity.

As shown in the review, no one has yet conducted experimental measurements of TPMS performance using a nanofluid. Thus, the uniqueness of this paper is its experimentation using nanofluids in the presence of a triply periodic minimal surface porous structure. Section 2 presents the experimental setup used in this work. Section 3 concentrates on the numerical modelling compared to the experimental data. The results are presented in Section 4. And finally, the conclusion is in Section 5.

2. Experimental Measurements

The experimental measurement conducted by Kerme et al. [17] was extended in the present article to a different fluid class: distilled water containing metallic particles. In this context, the fluid is called a nanofluid [11]. The concentration of nanofluid is 0.6%vol, and the presence of these nanoparticles increases the conductivity of the cooling fluid. The previous experiment by Kerme et al. [17] will be repeated with this new fluid class. The TPMS porous structure is made of two alloys: the first is $AlSi_{10}Mg$, and the second one is silver. It has been shown in the literature that the silver alloy exhibits a large thermal conductivity; thus, an improved heat enhancement is expected. The TPMS structure was designed and printed using a gyroid cell and had a porosity of 0.7.

Different flow rates were analyzed experimentally and at a constant heat flux. However, the inlet flow temperature varies from case to case and should be considered during the cooling performance evaluation. Thus, temperature measurement was conducted below the TPMS structure and at the flow inlet and outlet in the experiment. In addition to the nanofluid cooling liquid, distilled water was used for the two types of TPMSs. Thus, the cooling fluid was water and nanofluid.

2.1. Description of the Experiment

Figure 1 presents the experimental setup and the test section. A pump with a controlled flow rate was used to force fluid through the test section. The flow rate was selected to maintain laminar flow. Any gas bubble formation was removed before starting the experiment. The heat was generated using a voltmeter and ammeter, and the heat flux was fixed at 30,800 W/m^2. A water bath was used to maintain a low temperature at the entrance of the test section. However, some variation occurred due to the difficulties of maintaining identical inlet temperatures. A heated block made of aluminum located below the test section was used in the experiment. The thermocouples were 1 mm below the interface between the heated block and the test section. In total, nine thermocouples were used: one at the inlet, seven below the interface, and one at the outlet. The test section had the dimensions of an Intel Core i7 computer processor. The base was square, of 37.5 mm long, and the height was 12.7 mm. The aluminum heated block and the TPMS structure had identical dimensions. A data acquisition system was used to collect data at different time steps. More details about the experiment can be found in [8].

Figure 2 presents the test section with the aluminum TPMS and silver TPMS. As shown, the flow enters from one side of the hexagonal and exits from the opposite side. Fluid circulates through the structure and absorbs heat conducted from the heated block. Thermo-pasts are added between the TPMS structure and the heated block. The test section is made of isolating material to stop heat leakage.

A plastic sheet covered the top of the test section, and multiple screws were used to seal the top part of the test section.

As indicated earlier, five different flow rates were applied during the experiment. These were 3.74 cm^3/s, 7.86 cm^3/s, 11.8 cm^3/s, 15.73 cm^3/s, and 19.85 cm^3/s. The heat flux applied at the aluminum block remained constant at 30,800 W/m^2. The inlet temperature may vary slightly between runs, but the analysis measures and considers it. Figure 3 presents the timelapse for the case of the aluminum and silver structures. A nanofluid was

used in this representation, and thermocouple number 4 was chosen for this presentation. Thermocouple number 4 was approximately 16.8 mm from where the flow starts entering the test section. The inlet temperature, as seen, varied in each run, but a steady state was achieved after approximately 45 min.

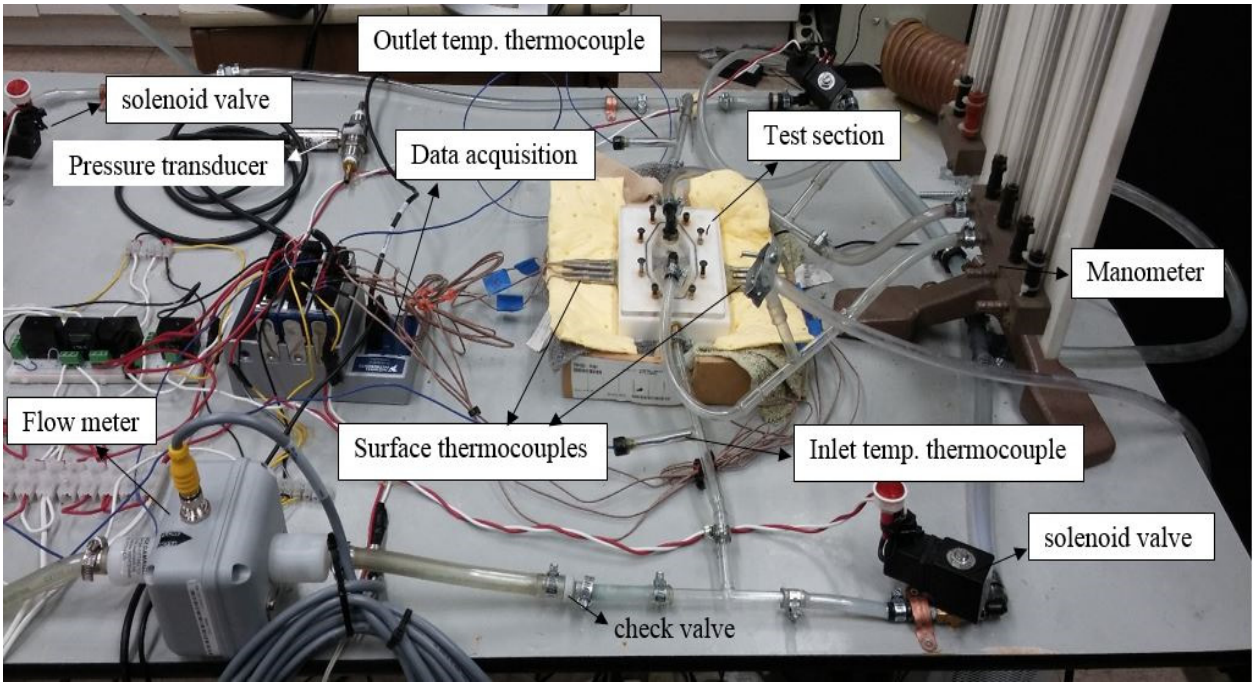
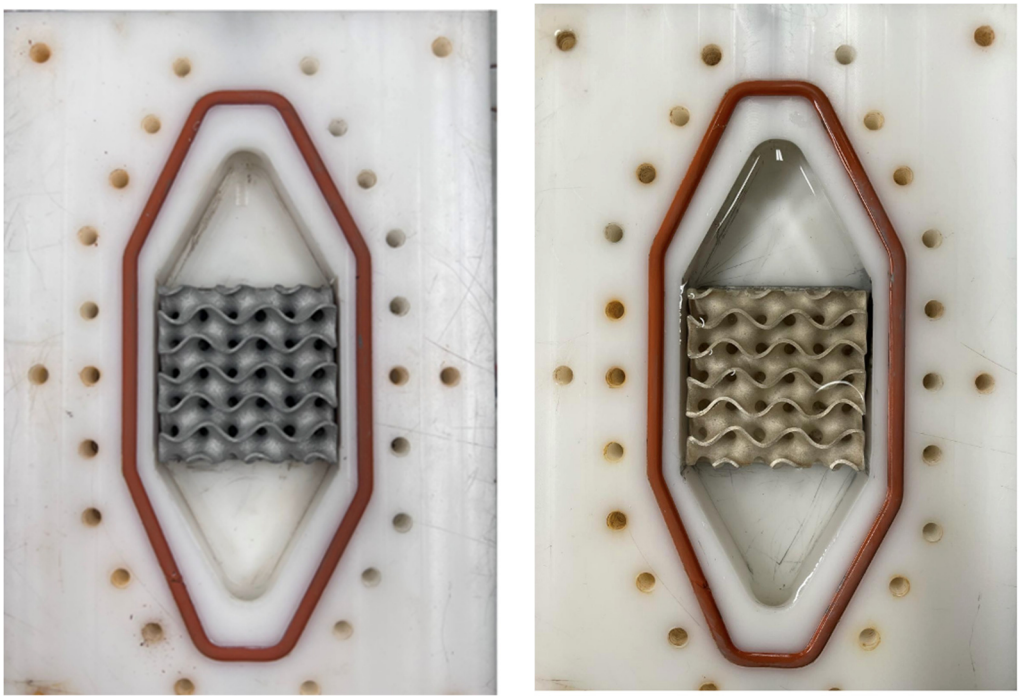


Figure 1. Experimental setup [1].



(**a**) (**b**)

Figure 2. Test section with the TPMS structure. (**a**) Aluminum TMPS in the test section. (**b**) Silver TPMS in the test section.

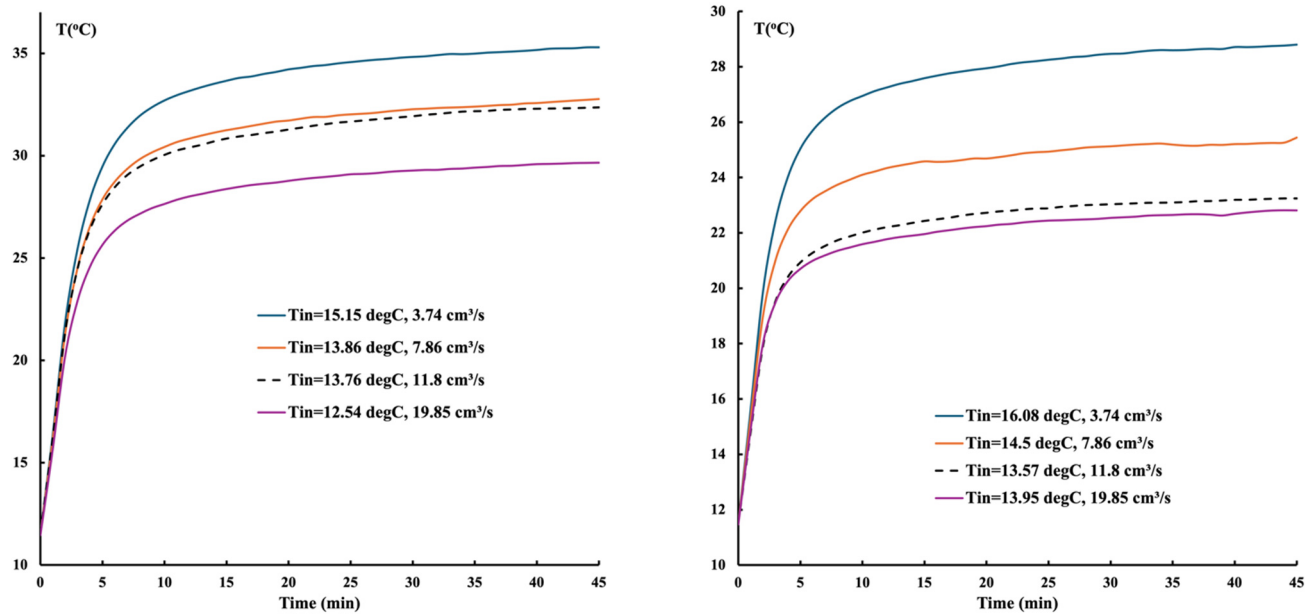


Figure 3. Temperature variation as a function of time. (**a**) Aluminum TPMS structure. (**b**) Silver TPMS structure.

As seen in Figure 3, the temperatures, regardless of the flow rate and the inlet temperature, reached a steady state approximately after 45 min. Data collection may take up to two hours as the inlet temperature needs to drop to a reasonable level for the next run to begin. A slight fluctuation in the temperature is also shown. The investigation led us to believe that this fluctuation was due to some current instability leading to heat flux fluctuation. However, it is noticeable that it was adjusted after all, and the temperature rose to the correct value. Because silver thermal conductivity is almost double that of aluminum, more heat is extracted from silver than from aluminum. The inlet temperature for all cases fluctuated by one degree between runs. Even if an attempt was made to start the experiment at precisely the identical inlet temperature, this was impossible to reach. However, the inlet temperature was taken into consideration in the analysis.

2.2. Uncertainty Analysis

An uncertainty analysis was conducted within the apparatus's components used in the experimental data collection. The error-propagating components of the device are the flowmeter and the T-type thermocouples. For the flowmeter, the error was determined, through the calibration processes, to be equal to 0.44% US gallon per minute (USGPM). The uncertainty was obtained through the calibration processes for the T-type thermocouple, yielding an uncertainty of 0.75% (°C). The uncertainty of the non-dimensional parameters, such as the Nusselt number and the temperature, was detected as the temperature and the flow rate fluctuate. For instance, the Nusselt number is expressed by

$$\mathrm{Nu} = \frac{\mathrm{h_x} \cdot \mathrm{D}}{\mathrm{k}_f} \tag{1}$$

and the Reynolds number is expressed by:

$$\mathrm{Re} = \frac{\mathrm{u_{in}} \cdot \mathrm{D}}{\nu} \tag{2}$$

Additionally, there exist several parameters that are dimensional, such as the local heat transfer coefficients expressed in W/m^2C expressed by:

$$h_x = \frac{q''}{T_x - Tin} = \frac{q''}{\Delta T_x} \quad (3)$$

As we can see, the calculations in all the cases above rely on the experimental results. The uncertainty of the average Nusselt number can be obtained as follows:

$$\delta Nu = \sqrt{\left(\frac{\partial Nu_x}{\partial x}\cdot\delta x\right)^2 + \ldots + \left(\frac{\partial Nu_x}{\partial y}\cdot\delta y\right)^2 + \ldots + \left(\frac{\partial Nu_x}{\partial z}\cdot\delta z\right)^2} \quad (4)$$

where h_x represents the local heat transfer coefficient over the heater surface, T_x represents the local surface temperature, T_{in} represents the water inlet temperature, D represents the inlet diameter of the tube, and u_{in} represents inlet water velocity throughout the test section. The kinematic viscosity of the fluid is ν, and k_f represents the thermal conductivity of water. The maximum value of the uncertainty of the local Nusselt number was 2.6%. Table 1 shows the physical properties of the fluids used in the experimental setup, such as the distilled water and the nanofluid.

Table 1. Physical properties of the materials and fluids used [17].

Fluids and Materials	ρ (kg/m^3)	μ (kg/m.s)	Cp (J/kg.K)	k (W/m.K)
Distilled Water	998.2	0.001001	4128	0.613
Nanofluid (0.6%vol Al_2O_3 + 99.4%vol water)	1013.811	0.00104	4109.198	0.6242

As observed in Table 1, the nanofluid generally has an increase in thermal conductivity, density, and heat capacity. On the other hand, the higher the viscosity coefficient, the higher the pressure drop, which will be examined in detail.

3. Finite Element Formulation

The numerical modelling was conducted using COMSOL software version 6. COMSOL uses the finite element method, and the segregated solver was used. The fluid was assumed to be Newtonian, and a steady-state condition was adopted. The reason for assuming Newtonian flow for the nanofluid was the low concentration of metallic nanoparticles. Table 1 presents the physical properties of the two fluids under consideration. The flow was assumed to be incompressible, and with the flow rate used, the flow was laminar.

The full Navier–Stokes equations combined with the continuity and energy equations were solved numerically. The TPMS was modelled as a solid structure in the flow domain. This approach made the model very complex. The reason is that one may observe channels with closed ends inside the structure. Thus, this requires the flow to be redirected to the place with lower pressure. One may observe some high flow inside the structure, then the flow decreases. This non-uniform flow allows the fluid to circulate longer inside the structure, removing additional heat. Regarding the solving of the equations, it makes solving this set of equations more challenging to converge. To overcome this situation, initially assuming zero flow, the fluid equations are solved first. The model is solved again upon achieving convergence using the flow field results as an initial condition. The new set of equations consists of the flow field formulation and the energy equation. This approach allows a fast and accurate convergence. The convergence criteria are set when the residue-containing variables, such as the three velocities, the pressure, and the temperature, are below 10^{-6}. In addition, the refined mesh can help to solve this problem accurately but at the expense of the processing time.

The formulations used in the current analysis were the following:

3.1. Navier–Stokes Formulation in the x Direction

$$\rho_f\left[u\frac{\partial u}{\partial x}+v\frac{\partial u}{\partial y}+w\frac{\partial u}{\partial z}\right]=-\frac{\partial p}{\partial x}+\mu_f\left[\frac{\partial^2 u}{\partial x^2}+\frac{\partial^2 u}{\partial y^2}+\frac{\partial^2 u}{\partial z^2}\right] \quad (5)$$

3.2. Navier–Stokes Formulation in the y Direction

$$\rho_f\left[u\frac{\partial v}{\partial x}+v\frac{\partial v}{\partial y}+w\frac{\partial v}{\partial z}\right]=-\frac{\partial p}{\partial y}+\mu_f\left[\frac{\partial^2 v}{\partial x^2}+\frac{\partial^2 v}{\partial y^2}+\frac{\partial^2 v}{\partial z^2}\right] \quad (6)$$

3.3. Navier–Stokes Formulation in the z Direction

$$\rho_f\left[u\frac{\partial w}{\partial x}+v\frac{\partial w}{\partial y}+w\frac{\partial w}{\partial z}\right]=-\frac{\partial p}{\partial z}+\mu_f\left[\frac{\partial^2 w}{\partial x^2}+\frac{\partial^2 w}{\partial y^2}+\frac{\partial^2 w}{\partial z^2}\right] \quad (7)$$

3.4. Energy Formulation

$$\rho_f Cp\left[u\frac{\partial T}{\partial x}+v\frac{\partial T}{\partial y}+w\frac{\partial T}{\partial z}\right]=k_f\left[\frac{\partial^2 T}{\partial x^2}+\frac{\partial^2 T}{\partial y^2}+\frac{\partial^2 T}{\partial z^2}\right] \quad (8)$$

In the model, the TPMS was made using a gyroid structure. The term gravity was removed since it is a forced convection condition, and gravity is neglected.

3.5. Boundary Conditions of the System

Figure 4 shows the boundary condition used in the model. It is worth mentioning that the heated block had a square base of 37.5 mm and a height of 12.7 mm. Similarly, the block containing the TPMS structure had the same dimensions. The inlet and the outlet cylinders had a diameter of 1 cm. The red arrows show where the heat flux was applied and had a constant value of 30,800 W/m^2. At the inlet, the fluid temperature as set as Tin; the applied inlet velocity was u_{in}, and the calculated temperature was T_{out} at the outlet. All the model boundaries except where the heat flux was applied were insulated and adiabatic walls were assumed. Thus, the boundary condition in equation form is:

(i) The velocity $u = u_{in}$ in the x direction is applied at the inlet.
(ii) At the inlet, the temperature of the fluid enters the test section at T = Tin.
(iii) At the outlet, an open boundary is applied where the stresses are equal to zero.
(iv) The bottom surface of the aluminum block is heated with a heat flux q″, as shown in red.
(v) All external surfaces are assumed to be adiabatic, $\frac{\partial T_{Surface}}{\partial n}=0$, and for the flow, no-slip boundary conditions are applied.

Multiple parameters were evaluated to assess the importance of this structure in heat removal. The current model's porosity was set at 0.7 when this structure was designed. The permeability was not known but did not need to be investigated since, in the model, the TPMS was modelled physically as a solid structure. The first important parameter to evaluate was the heat convection coefficient, known as

$$h=\frac{q''}{(T-Tin)} \quad (9)$$

where the ratio of the applied flux is divided by the temperature difference between the calculated one and the inlet temperature. The calculated one was measured 1 mm below the interface in the solid aluminum block. The local Nusselt number was thus defined as

$$Nu=\frac{hD}{k_f} \quad (10)$$

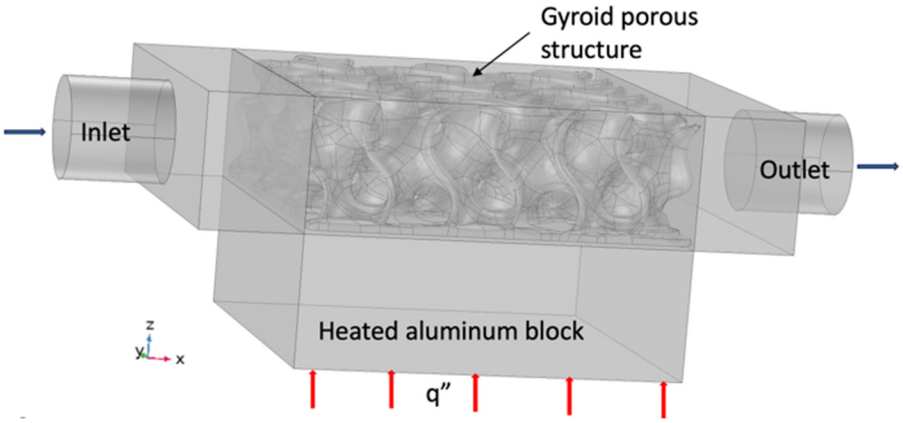


Figure 4. Boundary conditions used in the model.

The pressure drop plays a crucial role in the design of a cooling system. This is represented by the friction factor, which is defined as:

$$f = \frac{0.5\Delta pD}{\rho L u_{in}^2} \tag{11}$$

It is interesting to combine the thermal and the hydraulic effects by evaluating the performance evaluation criteria (PEC), defined as

$$PEC = \frac{\text{local Nu}}{f^{\frac{1}{3}}} \tag{12}$$

The above set of equations was obtained from [8]. These non-dimensional parameters were assessed during the analysis. A mesh sensitivity analysis was conducted to ensure the accuracy of the model. An average mesh level, which consisted of 1,338,201 elements, was adopted. These elements were composed of tetrahedral elements and boundary elements. This optimum mesh was obtained after multiple mesh size selections. The criteria for selecting the optimum mesh was evaluating the Nusselt number. When the Nusselt number between two consecutive mesh sizes is less than 1%, we assumed that the mesh is optimum.

4. Results and Discussion

Multiple experiments were conducted with different cooling fluids, flow rates, and porous structures. Water was first used as the cooling fluid, and the temperature measurement was performed for various flow rates. An aluminum TPMS structure and silver TPMS structure were used in this experiment. As discussed earlier, the inlet temperature varied between experiments but could be adjusted by presenting the difference between the measured and inlet temperatures. Figure 5 displays the data from the experiment with water as the flowing liquid in the aluminum TPMS structure. Figure 5a presents the temperature distribution measured 1 mm below the TPMS/heated block interface. As observed and evident, the cooling process removes more heat from the system as the flow rate increases. An additional observation worth mentioning is the uniformity of the temperature distribution. This uniform temperature distribution is an important finding using TMPS. The temperature difference between thermocouples #1 and #7 does not exceed two degrees, regardless of the inlet temperature. As the flow rate increases, the temperature uniformity improves. Also, in this experiment, the inlet temperature range between the low and highest flow rates is approximately 12.5 degrees Celsius.

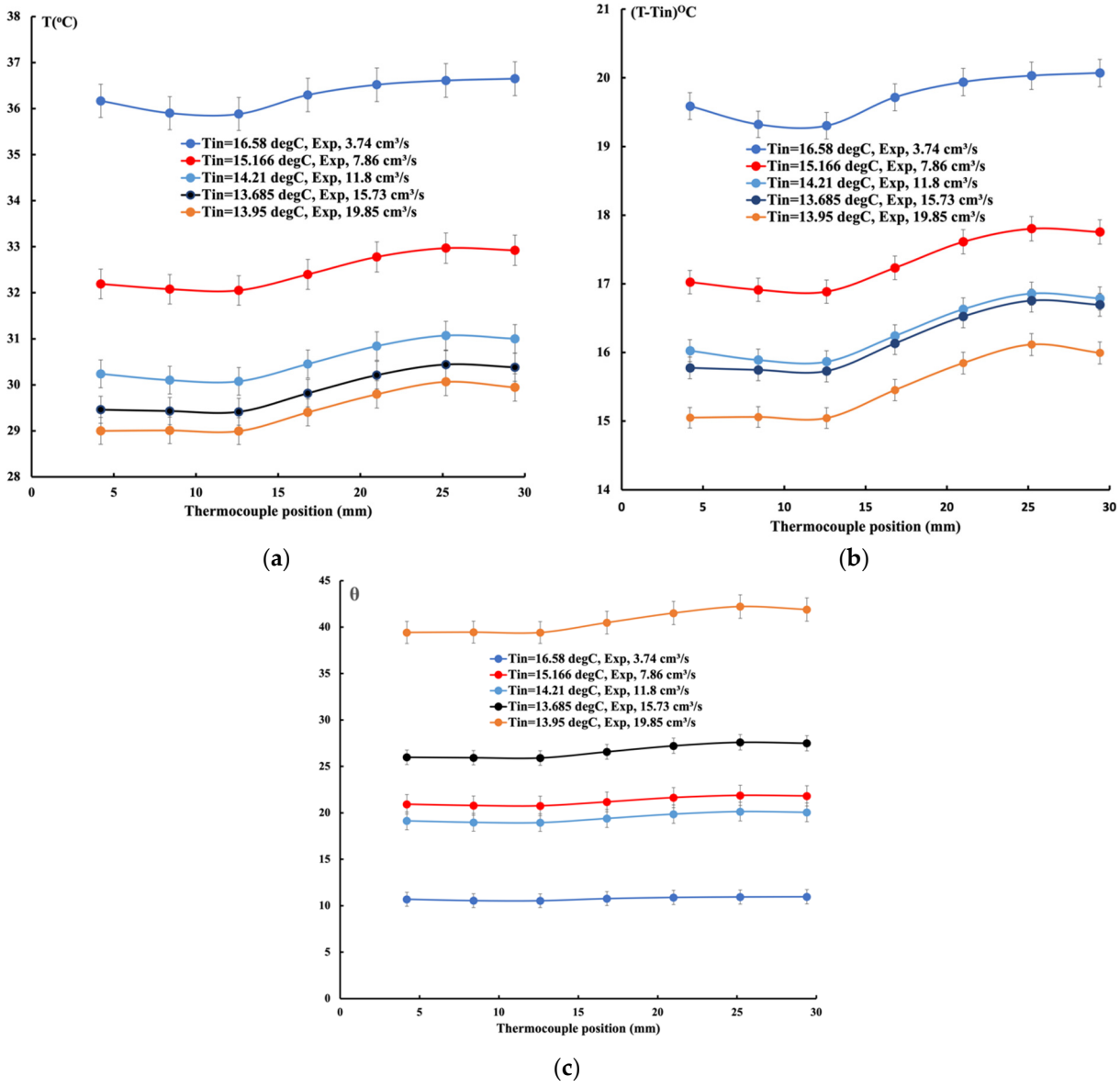


Figure 5. Temperature measurement for water as the cooling fluid through an aluminum TPMS structure. (**a**) Temperature distribution, (**b**) temperature difference, and (**c**) non-dimensional temperature.

Figure 5b shows the temperature difference between the measured one and the inlet temperature to observe the amount of heat removed by the TPMS regardless of the inlet temperature. In this graph, the temperature scale is changed to verify the uniformity of the temperature accurately. The uniformity and the temperature difference, as observed in Figure 5a, is around 1.25 degrees Celsius. This uniformity is detected regardless of the inlet temperature. However, another variable measured experimentally is worth mentioning: the outlet temperature. Figure 5c displays the non-dimensional temperature measured experimentally, combining the inlet and outlet temperatures with the measured temperature T.

In this case, as shown in Figure 5c, it is evident that the temperature is uniform by removing the effect of the different inlet and outlet temperatures. The experiment was repeated by replacing the aluminum TPMS structure with a silver TPMS structure. It is known that silver has a high thermal conductivity. That means more heat is absorbed by the structure and taken away with the water circulation.

Figure 6 presents the case of the silver structure. By examining Figure 6a, it is found that the temperature is lower than the one presented in Figure 5a. The thermal conductivity

effects of the structure play an important role in heat extraction. Again, suppose we continue the comparison between Figures 5a and 6a. In that case, the temperature variation for the flow rate of 7.86 cm^3/s exhibits a higher temperature measurement than that for a flow rate of 3.74 cm^3/s. The reason for that is the inlet temperature at a low flow rate is higher than at the flow rate of 7.86 cm^3/s. Thus, by analyzing Figure 6b and, consequently, Figure 5b, the effect of inlet temperature is removed, and it shows that, as the flow rate is low, the temperature is high and is reduced as the flow rate increases. Figure 6c displays the non-dimensional temperature by considering the inlet and outlet temperatures. Temperature uniformity is maintained, proving that the TPMS structure provides a more uniform heat distribution.

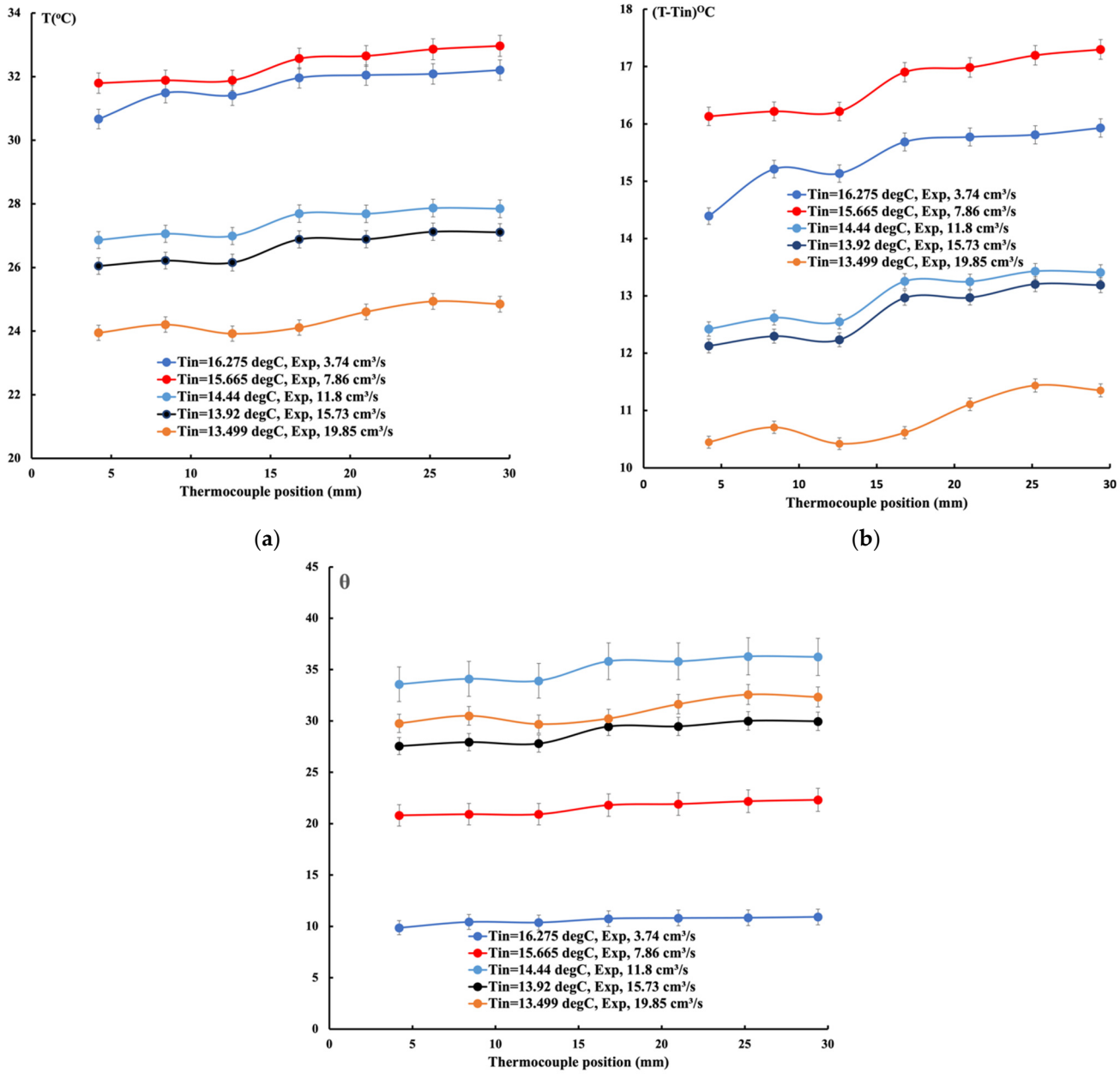


Figure 6. Temperature measurement for water as the cooling fluid through the silver TPMS structure. (**a**) Temperature distribution, (**b**) temperature difference, and (**c**) non-dimensional temperature.

Figure 7 displays the measured temperature distribution with the nanofluid as the flowing liquid using the aluminum TPMS structure. The first observation one may notice is the drop in temperature since the nanofluid has a higher thermal conductivity, as shown in Figure 7a. Moreover, as shown in Figure 7b, one may notice a heat enhancement as the flow rate increases by removing the inlet temperature. Still, the temperature difference between two different flow rate measurements is lower than when water was the cooling fluid. That means one can achieve an acceptable low heat removal at a low flow rate, thus reducing the effect of the pressure drop.

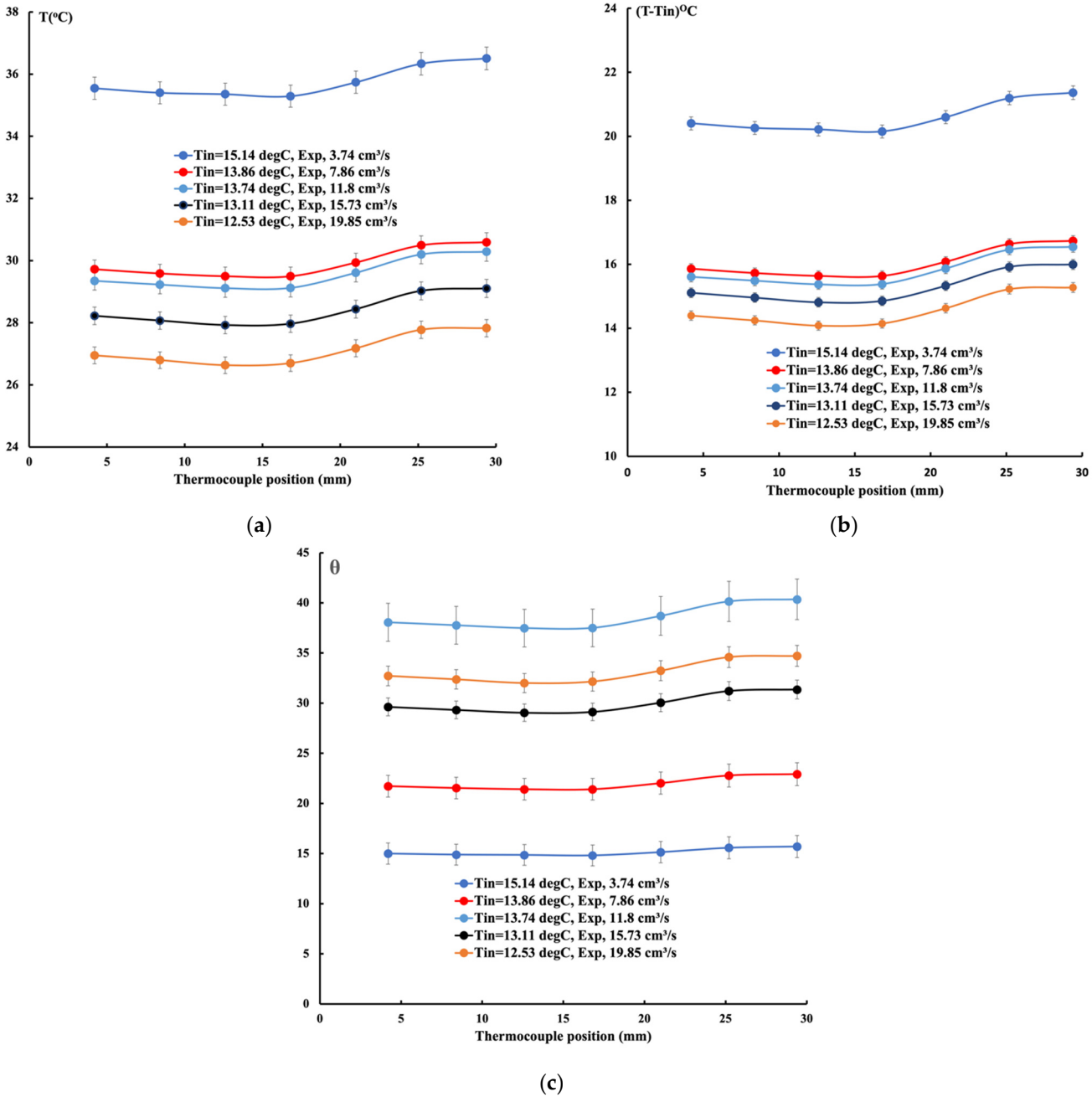


Figure 7. Temperature measurement with the nanofluid and the aluminum TPMS structure. (**a**) Temperature measurement, (**b**) temperature difference, and (**c**) non-dimensional temperature.

Furthermore, Figure 7c indicates the importance of the nanofluid in achieving a uniform temperature distribution. As shown in Figure 7c, a precise uniform temperature

distribution is detected for all flow rates. This temperature profile is ideal for a uniform cooling system at low pressure drop (i.e., low flow rates).

Figure 8 displays the temperature measurement using the silver structure and nanofluid. A similar observation to that in Figure 7 is obtained in this case. The uniformity of the temperature distribution and effectiveness in removing heat at low flow rates were the highlights of this experiment. In addition, a lower temperature was measured due to the higher thermal conductivity of the silver TPMS structure.

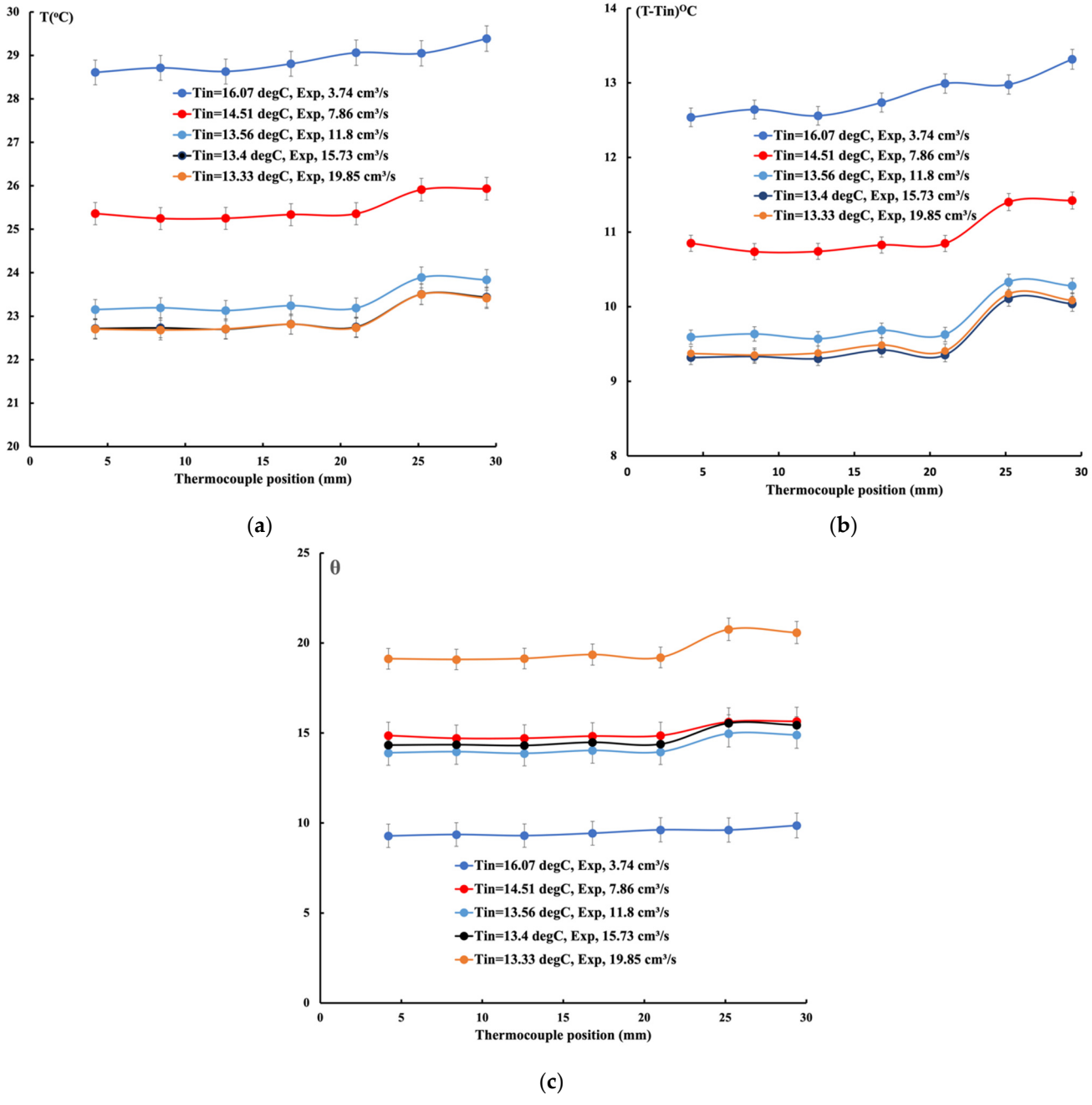


Figure 8. Temperature measurement with the nanofluid and silver TPMS structure. (**a**) Temperature measurement, (**b**) temperature difference, and (**c**) non-dimensional temperature.

4.1. Comparison between Experimental Measurements and Numerical Data

Two different liquids were used to circulate in the TPMS structure. These were distilled water and a nanofluid, which was distilled water containing 0.6%vol of aluminum nanoparticles. These particles were approximately 32 nm in diameter.

4.1.1. Water as the Cooling Fluid

Using the COMSOL software, the model was solved using the finite element methods. Some boundary conditions were adopted from the experimental measurement, such as the inlet temperature, flow rate, and applied heat flux. With those boundary conditions, the model was solved for different numerical conditions, and results were compared with the experimental data. Using the numerical data, the experimental temperature measurement and the numerical calculated value were compared, as shown in Figure 9, for water as the circulating fluid.

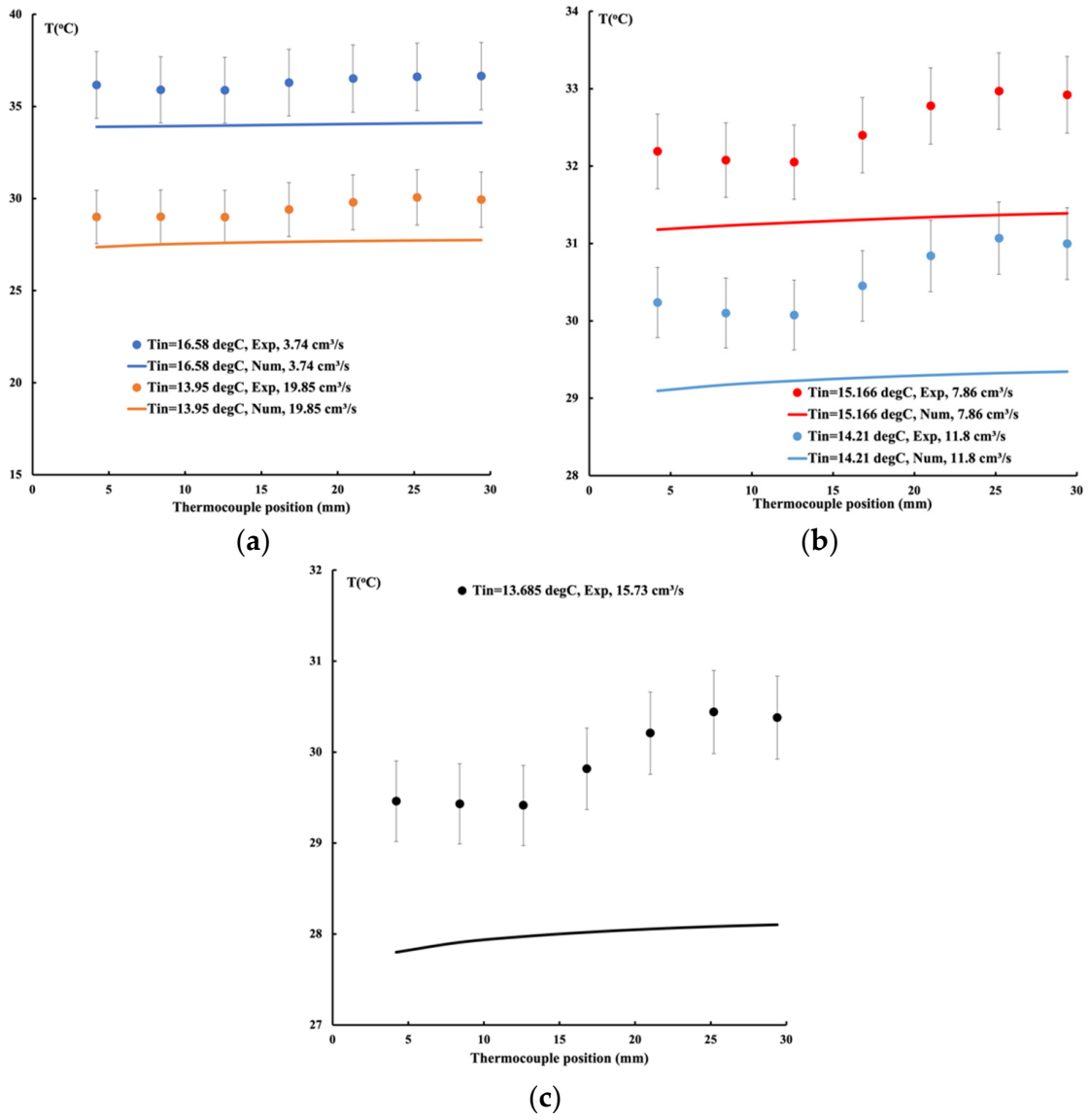


Figure 9. Comparison of the temperature between the numerical and experimental measurements (aluminum TPMS and water) (**a**) Flow rate 3.74 cm^3/s and 19.85 cm^3/s (**b**) flow rate 7.86 cm^3/s and 11.8 cm^3/s, (**c**) flow rate 15.73 cm^3/s.

As shown, a good agreement between the two measurement sets was achieved. The slight variation in the experimental measurement was trivial and expected. The difference between the two datasets could be due to heat flux fluctuation, heat losses, or inlet flow fluctuation. The difference between the experimental and numerical datasets was less than 2 °C. Figure 10 compares water as a cooling fluid using the silver TPMS.

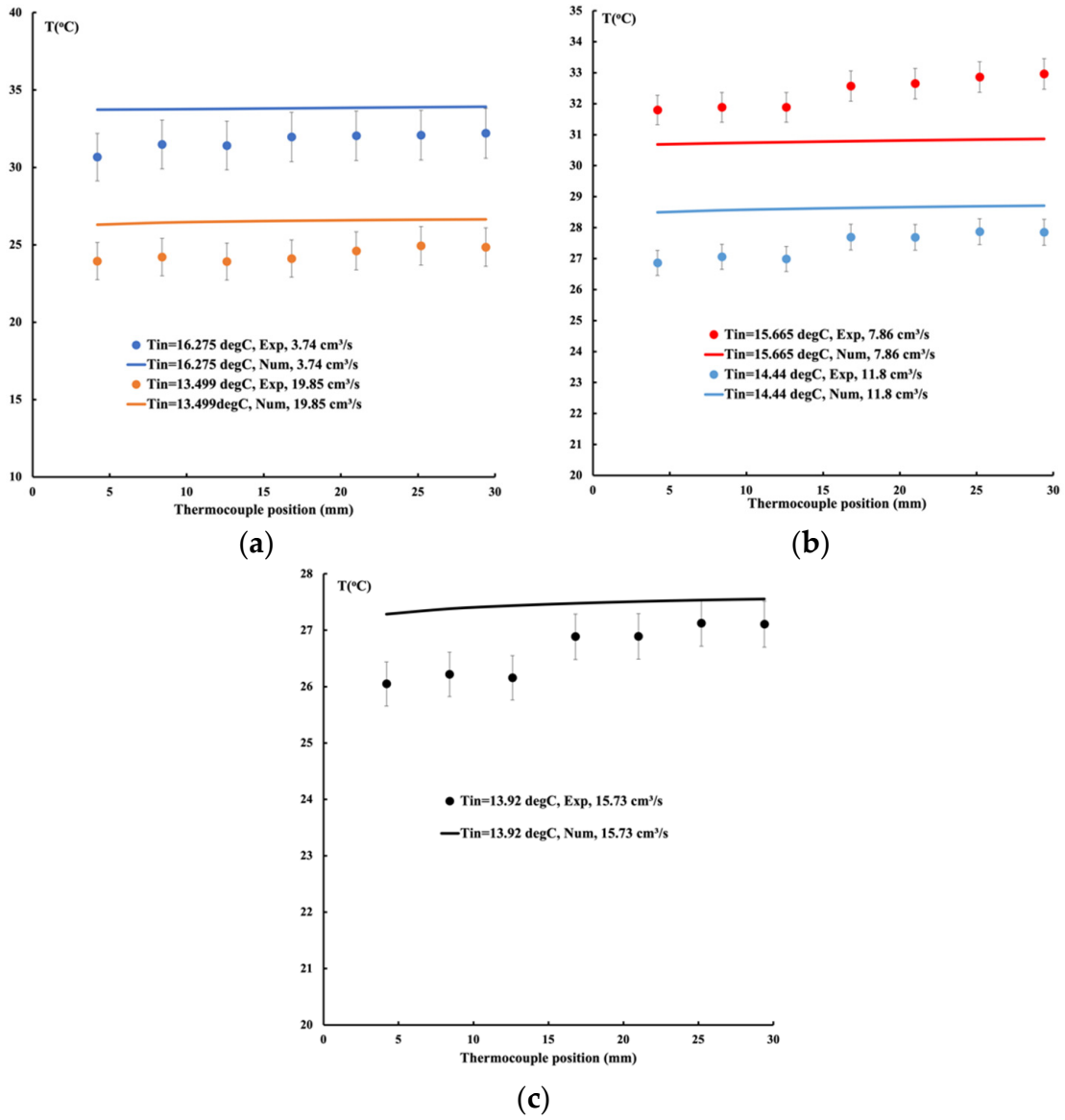


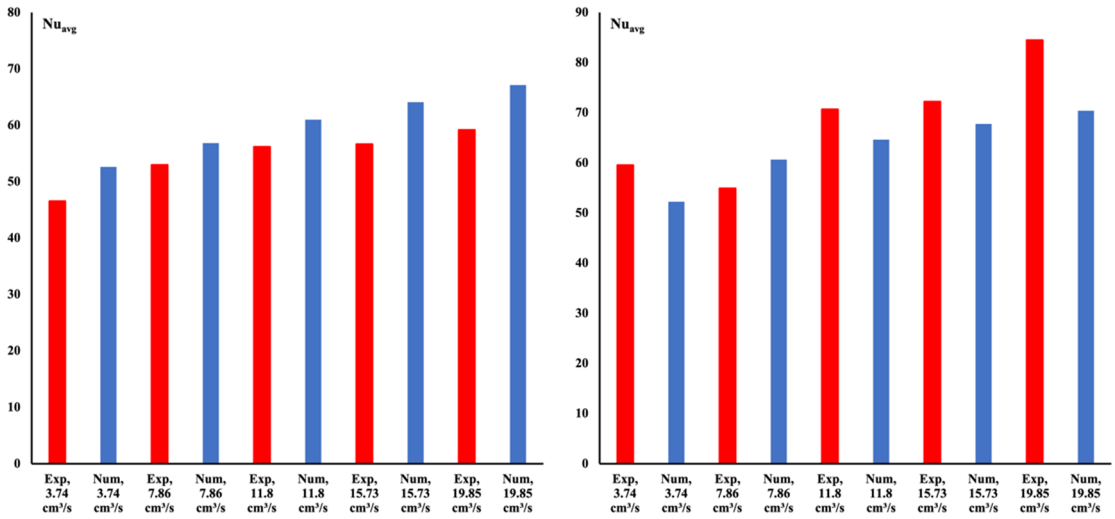
Figure 10. Comparison of the temperature between the numerical and experimental measurements (silver TPMS and water). (**a**) Flow rate 3.74 cm^3/s and 19.85 cm^3/s (**b**) flow rate 7.86 cm^3/s and 11.8 cm^3/s, (**c**) flow rate 15.73 cm^3/s.

A similar comparison agreement was observed for the case of the aluminum TPMS but at lower temperatures. Figures 9 and 10 show that the numerical modelling results differ slightly from the experimental results. This is due to some heat losses in the experiment, even with perfect insulation; thus, slightly lower experimental results were achieved.

The differences between the experimental and numerical results are shown in Table 2. The difference between experimental and numerical results is reasonable and well justified. The Nusselt number explained in Equation (10) represents the best heat removal indicator. Figure 11a illustrates the comparison when the TPMS structure is aluminum, and Figure 11b shows an identical case when the TPMS structure is silver. There is a good agreement between the two sets of Nusselt numbers. It is essential to note that, for the case of the aluminum structure, the numerical data show a slightly higher value than the experimental data at high flow rates. This may be due to heat losses occurring during the experiment.

Table 2. Temperature differences between the experimental measurement and computed numerical calculation (water cooling fluid).

Difference (%)	TC#1	TC#2	TC#3	TC#4	TC#5	TC#6	TC#7	Average
Al, 3.74 cm^3/s	6.28	5.49	5.33	6.30	6.75	6.88	6.89	6.28
Al, 7.86 cm^3/s	3.14	2.64	2.43	3.36	4.38	4.85	4.65	3.63
Al, 11.8 cm^3/s	3.77	3.08	2.83	3.89	5.00	5.61	5.33	4.22
Al, 15.73 cm^3/s	5.64	5.17	4.90	6.02	7.13	7.74	7.49	6.30
Al, 19.85 cm^3/s	5.63	5.16	4.83	5.96	7.05	7.78	7.34	6.25
Ag, 3.74 cm^3/s	9.99	7.20	7.57	5.82	5.66	5.64	5.34	6.75
Ag, 7.86 cm^3/s	3.50	3.63	3.52	5.45	5.60	6.13	6.36	4.88
Ag, 11.8 cm^3/s	6.07	5.55	5.98	3.41	3.53	2.95	3.09	4.37
Ag, 15.73 cm^3/s	4.75	4.43	4.89	2.20	2.30	1.51	1.64	3.10
Ag, 19.85 cm^3/s	9.84	9.20	10.79	10.11	8.06	6.75	7.20	8.85



(**a**) (**b**)

Figure 11. Experimental and numerical averages of the Nusselt number. (**a**) Aluminum TPMS structure. (**b**) Silver TPMS structure.

On the other hand, the results for the silver TPMS structure show that the higher value of the experiment may be due to a fluctuation in the heat flux. Even a one-degree change in the temperature can lead to a more significant change in the Nusselt number. However, the agreement is generally good, with an increase in the Nusselt number as the flow rates increase accordingly.

An important parameter that combines the thermal and hydraulic effects is the performance evaluation criterion, obtained using Equation (12). In the experimental side, no measurement was taken for the pressure drop; so, one can rely only on the numerical PEC, as shown in Figure 12.

By closely examining Figure 12, one can immediately identify the silver TPMS structure as the best structure for heat removal in engineering applications. The pressure dropped for both cases, or the friction factor was the same since the structure design was identical and for a similar flow rate. However, the performance evaluation criterion was higher in magnitude since the silver structure had a higher Nusselt number. In addition, as the flow rates increased, the performance evaluation criterion also increased.

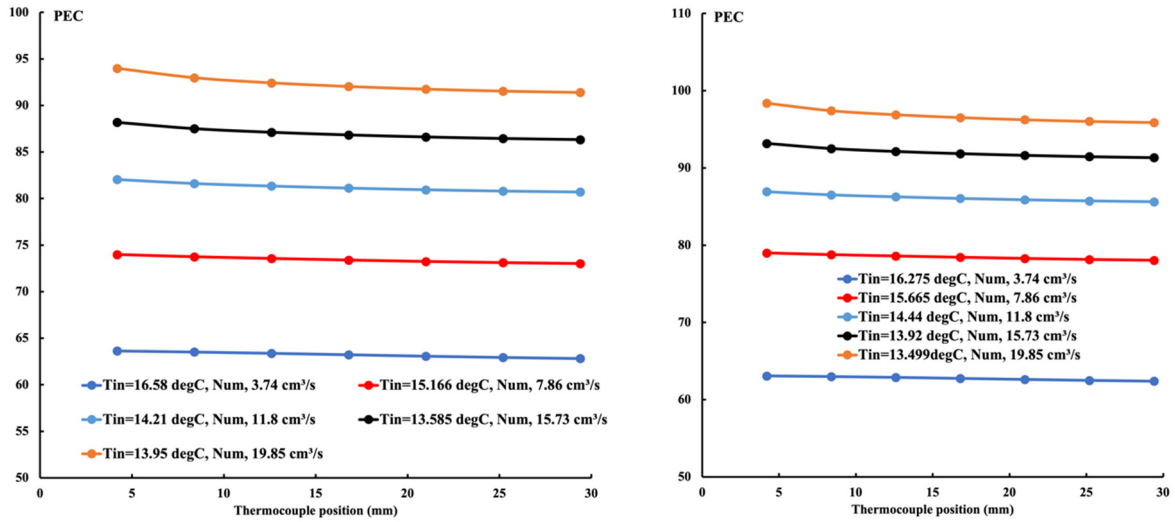


Figure 12. Performance evaluation criterion for the two cases: (**a**) aluminum TPMS structure and (**b**) silver TPMS structure.

4.1.2. Nanofluid as the Cooling Fluid

Previous work by the authors of this paper used a nanofluid to study channel heat enhancement [18]. In the current paper, the nanofluid was mixed using a sonic mixture before being used in the experiment. Also, it is essential to indicate that, after each experiment, the system was flushed with distilled water to remove all the metallic particles from the piping system. The TPMS porous structure was also carefully cleaned to avoid solidifying the nanoparticles in the channel of the structure. Figures 7 and 8 experimentally present the temperature distribution measured by the thermocouple for the same flow rate as the previous case in the presence of the aluminum and silver TPMS structures.

The first observation worth mentioning and confirmed earlier with fluid circulation is that the silver TPMS structure helps in heat removal better than the aluminum structure. As shown in Figures 7a and 8a, a lower temperature is detected in the presence of the silver structure. Furthermore, by examining Figures 7c and 8c against Figures 5c and 6c, one may notice that, by eliminating the inlet and outlet temperature from the data, the nanofluid provided better cooling than the distilled water case. It is essential to indicate that the inlet nanofluid varied between each run; thus, studying the variable θ is the right approach. In addition, nanofluid maintains temperature uniformity, proving to us that the structure design led to this uniformity.

Figure 13 compares the measured experimental data and the calculated numerical temperature. One notices a good agreement between the two datasets, and the differences presented in Table 2 for water as the circulating fluid are very close to the differences in Figure 13 when the nanofluid is the circulating fluid. However, it will be interesting to investigate the nanoparticles' agglomeration and path inside the structure. This could be conducted numerically and will be the subject of future investigation. The authors believe this is the first case of a nanofluid experimentally conducted inside a TPMS structure. Figure 13d–f shows that the difference between the computed and measured data is significant compared to all other cases. The main reason for these discrepancies, based on experience, may be an error in the flow rate measurement. It is noticeable that, sometimes, the nanoparticles create a false reading for the flow rate due to some accumulation in the pump. The second reason is that the fluctuation of electric current may provide a lower heat flux, leading to lower temperatures. This issue will be addressed in a different article. The variation trend is reasonable between the two sets of data.

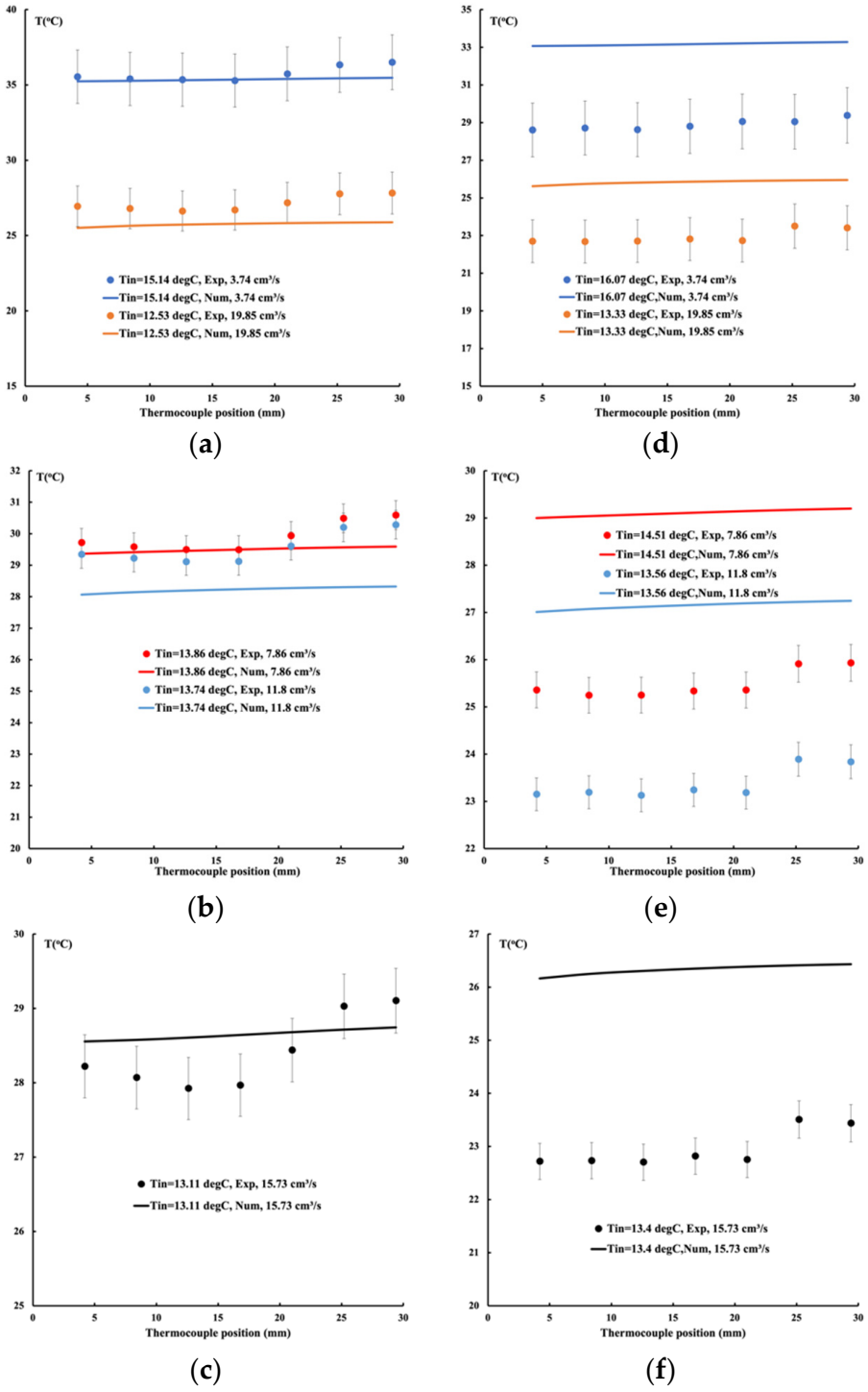


Figure 13. Temperature comparison between the experimental measurement and numerical calculation using the nanofluid. (**a**) Temperature distribution along the aluminum-heated block. (**b**) Temperature difference with the aluminum structure. (**c**) Non-dimensional temperature with the aluminum structure. (**d**) Temperature distribution along the silver-heated block. (**e**) Temperature difference with the silver structure. (**f**) Non-dimensional temperature with the silver structure.

The uniformity of the temperature distribution is worth mentioning. The temperature slope was evaluated numerically and experimentally. Figure 14 shows the changes in the slope for the two cases for all flow rates. It is noticeable that the silver structure exhibits a lower slope when compared to the aluminum structure. In addition, the slope value is very low for both cases, which is a good indicator of the uniformity of the cooling process.

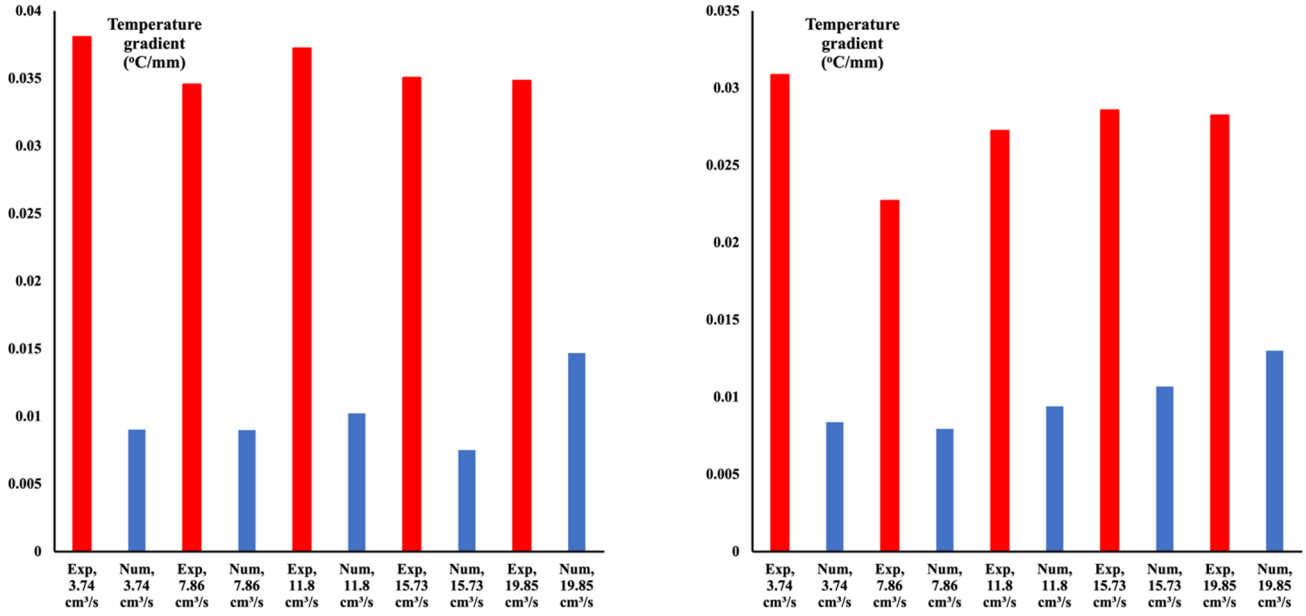


Figure 14. Temperature variation for different flow rates using the nanofluid. (**a**) Aluminum structure. (**b**) Silver structure.

The performance evaluation criteria for the nanofluid case were calculated. As shown in Figure 15, it is expected that silver structures exhibit a higher PEC when compared to the aluminum ones; however, in both cases, in the presence and the absence of the nanofluid, both water and the nanofluid exhibit similar performance evaluation criteria. The reason is that the nanofluid can achieve a better heat enhancement but at the expense of reducing the pressure drop.

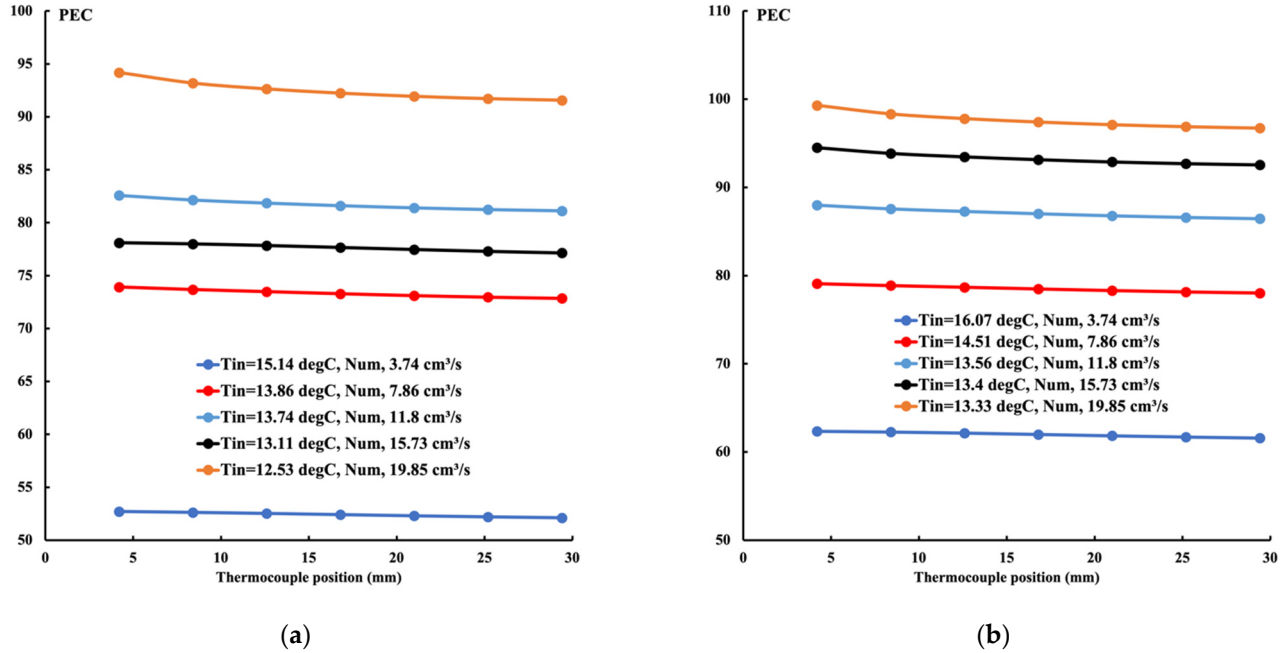


Figure 15. Performance evaluation criteria in the presence of the nanofluid. (**a**)Aluminum TPMS structure. (**b**) Silver TPMS structure.

5. Conclusions

Triply periodic minimal surfaces (TPMSs) have shown great potential as porous structures in different engineering applications. Amongst them is the cooling heat sink, which is the subject of this paper. The advantage of such a structure is the ability to design it based on the applications. For biomedical applications, the interest is in the strength of the structure to replace any bone in the body. In thermal management, it is lightweight and could provide good heat removal. The present paper used a TPMS to study its effectiveness in heat removal. Two different Newtonian fluids, water and a nanofluid, were used, with a concentration of 0.6% nanoparticles. The experiments were conducted for various flow rates, inlet temperature conditions, and two different TPMS structures, aluminum and silver, by maintaining a constant heat flux. The TPMS structure was a gyroid, having a porosity of 0.7. The experimental measurements were compared to the finite element technique's numerical results. The results achieved in this paper demonstrate that:

1. TPMS is a suitable porous structure that exhibits excellent heat removal with a reasonable pressure drop. The pressure drop may vary depending on the structure design.
2. Since wavy and straight channels generally help with heat extraction by maintaining low pressure drops, TPMSs could be designed to contain channels in the structure.
3. Heat distribution was uniformly distributed; thus, no boundary layer formation was detected. This is an essential finding for removing the boundary layer and allowing the heat to be absorbed by the moving fluid.
4. The thermal conductivity of the TPMS plays an additional role in enhancing heat transfer in the system. However, the material used for TPMSs also plays a significant role in heat enhancement.
5. The nanofluid, having a higher thermal conductivity, can improve heat removal but at the expense of the pressure drop. The performance evaluation criteria were higher when the silver TPMS was used.
6. The Nusselt number exhibits a higher value in the nanofluid's presence due to the fluid's greater thermal conductivity.
7. The performance evaluation criteria was found to be greater for the nanofluid compared to water. This is due to the higher Nusselt number.
8. Although the nanofluid exhibits a higher Nusselt number at the expense of a higher pressure drop, special attention must be paid to the nanoparticle agglomeration inside the void in the application.

Due to the lack of experimental measurements using TPMSs, this paper should be used as a benchmark for enhancing numerical models in general.

Author Contributions: Conceptualization, M.Z.S. and G.A.K. methodology, M.Z.S.; software, M.Z.S.; validation, M.Z.S.; formal analysis, M.Z.S. and G.A.K.; investigation, M.Z.S.; resources, M.Z.S.; All authors have read and agreed to the published version of the manuscript.

Funding: The authors acknowledge the financial support of NSERC, grant number RGPIN-2020-07021.

Institutional Review Board Statement: Not applicable.

Informed Consent Statement: Not applicable.

Data Availability Statement: The original contributions presented in the study are included in the article, further inquiries can be directed to the corresponding author.

Conflicts of Interest: The authors declare no conflicts of interest.

Nomenclature

Δp	Pressure difference (N/m^2)	ρ_f	Fluid density
T	Temperature in °K	μ_f	Fluid viscosity
Tin	Inlet temperature (°K)	Cp	Fluid specific heat

u_{in}	Inlet velocity (m/s)	k_f	Fluid conductivity
Nu	Local Nusselt number	h	Local heat transfer coefficient ($W/m^2.K$)
D	Inlet cylinder diameter (m)	q''	Heat flux applied to the bottom of the aluminum block ($W/m^2.K$)
p	Pressure (N/m^2)	u, v, w	Velocity in the x, y, and z directions (m/s)
T_{out}	Outlet temperature (°K)	PEC	Performance evaluation criterion
L	TPMS length (m)	$\theta = \frac{T-Tin}{T_{out}-Tin}$	Non-dimensional temperature
TC	Thermocouple		

References

1. Dutkowski, K.; Kruzel, M.; Rokosz, K. Review of the state-of-the-art uses of minimal surfaces in heat transfer. *Energies* **2022**, *15*, 7994. [CrossRef]
2. Abueidda, D.W.; Abu Al-Rub, R.K.; Dalaq, A.S.; Lee, D.-W.; Khan, K.A.; Jasiuk, I. Effective conductivities and elastic moduli of novel foams with triply periodic minimal surfaces. *Mech. Mater.* **2016**, *95*, 102–115. [CrossRef]
3. Al-Ketan, O.; Abu Al-Rub, R.K. Multifunctional Mechanical Metamaterials Based on Triply Periodic Minimal Surface Lattices. *Adv. Eng. Mater.* **2019**, *21*, 1900524. [CrossRef]
4. Yang, L.; Han, C.; Wu, H.; Hao, L.; Wei, Q.; Yan, C.; Shi, Y. Insights into unit cell size effect on mechanical responses and energy absorption capability of titanium graded porous structures manufactured by laser powder bed fusion. *J. Mech. Behav. Biomed. Mater.* **2020**, *109*, 103843. [CrossRef] [PubMed]
5. Tijing, L.D.; Dizon, J.R.C.; Ibrahim, I.; Nisay, A.R.N.; Shon, H.K.; Advincula, R.C. 3D printing for membrane separation, desalination and water treatment. *Appl. Mater. Today* **2020**, *18*, 100486. [CrossRef]
6. Peng, H.; Gao, F.; Hu, W. *Design, Model, and Characterize Triply Periodic Minimal Surface Heat Exchangers with Additive Manufacturing*; University of Texas at Austin: Austin, TX, USA, 2019.
7. Baobaid, N.; Ali, M.I.; Khan, K.A.; Abu Al-Rub, R.K. Fluid flow and heat transfer of porous TPMS architected heat sinks in free convection environment. Case Stud. *Therm. Eng.* **2022**, *33*, 101944.
8. Saghir, M.Z.; Kerme, E.D.; Hajialibabei, M.; Rasheed, H.; Welsford, C.; Al-Ketan, O. Study of the Thermal and Hydraulic Performance of Porous Block versus Gyroid Structure: Experimental and Numerical Approaches. *Energies* **2024**, *17*, 861. [CrossRef]
9. Moradmand, M.M.; Sohankar, A. Numerical and experimental investigations on the thermal-hydraulic performance of heat exchangers with Schwarz-P and gyroid structures. *Int. J. Therm. Sci.* **2024**, *197*, 108748. [CrossRef]
10. Hu, J.; Hu, K.; Zhang, Y.; Yang, X.; Wu, S. Experiment and simulation investigation of flow characters in metal foam. *Numer. Heat Transf. Part B Fundam.* **2022**, *83*, 24–38. [CrossRef]
11. Alqarni, M.M.; Ibrahim, M.; Assiri, T.A.; Saeed, T.; Abd Allah, A.M.; Ali, V. Two-phase simulation of a shell and tube heat exchanger filled with hybrid nanofluid. *Eng. Anal. Bound. Elem.* **2023**, *146*, 80–88. [CrossRef]
12. Eshgarf, H.; Nadooshan, A.A.; Raisi, A. A review of multi-phase and single-phase models in the numerical simulation of nanofluid flow in heat exchangers. *Eng. Anal. Bound. Elem.* **2023**, *146*, 910–927. [CrossRef]
13. Tang, W.; Zhou, H.; Zeng, Y.; Yan, M.; Jiang, C.; Yang, P.; Li, Q.; Zhao, Y. Analysis of the convective heat transfer process and performance evaluation of Triply Periodic Minimal Surface (TPMS) based on Diamond, Gyroid and Iwp. *Int. J. Heat Mass Transf.* **2023**, *201*, 123642. [CrossRef]
14. Ho, C.J.; Peng, J.K.; Yang, T.F.; Rashidi, S.; Yan, W.M. On the assessment of the thermal performance of microchannel heat sink with nanofluid. *Int. J. Heat Mass Transf.* **2023**, *201*, 123572. [CrossRef]
15. Rathore, S.S.; Mehta, B.; Kumar, P.; Asfer, M. Flow characterization in triply periodic minimal surface (TPMS)-based porous geometries: Part 1—Hydrodynamics. *Transp. Porous Media* **2023**, *146*, 669–701. [CrossRef]
16. Vahedi, M.; Mollaei Barzi, Y.; Firouzi, M. Two-phase simulation of nanofluid flow in a heat exchanger with grooved wall. *J. Therm. Anal. Calorim.* **2021**, *146*, 1297–1321. [CrossRef]
17. Kerme, E.D.; Hajialibabaei, M.; Saghir, M.Z.; El-Ketan, O. Experimental investigation of porous gyroid structure: Effect of cell size and porosity on performance. *Therm. Sci. Eng. Prog.* **2024**, *53*, 102728. [CrossRef]
18. Hajialibabaei, M.; Saghir, M.Z.; Dincer, I.; Bicer, Y. A Thermal Performance Improvement Study on a Novel Heat Sink Design. In *Advanced in Heat Transfer*; Elsevier: Amsterdam, The Netherlands, 2025; Volume 59.

Disclaimer/Publisher's Note: The statements, opinions and data contained in all publications are solely those of the individual author(s) and contributor(s) and not of MDPI and/or the editor(s). MDPI and/or the editor(s) disclaim responsibility for any injury to people or property resulting from any ideas, methods, instructions or products referred to in the content.